Optical properties of DAST in the THz range

Paul D. Cunningham[1,2,3] and L. Michael Hayden[1,4]

[1]Department of Physics, University of Maryland Baltimore County, Baltimore, Maryland 21250, USA
[2]Currently with the Naval Research Laboratory, Washington, DC 20375, USA
[3]paul.cunningham.ctr@nrl.navy.mil
[4]hayden@umbc.edu

Abstract: We report the far-infrared properties of the organic crystal DAST, a popular terahertz emitter, from 0.6 – 12 THz through use of a THz spectrometer incorporating air-plasma THz generation and electro-optic (EO) sampling in a poled EO polymer. We identify absorption features at 1.1, 3.1, 5.2, 7.1, 8.4, 11, and 12.3 THz and at 1.1, 1.3, 1.6, 2.2, 3, 5.2, 7.2, 9.6 and 11.7 THz for *a*-axis and *b*-axis polarized THz radiation respectively. These results allow for more accurate prediction of the optimum crystal thickness for broadband THz emission via optical rectification and difference frequency generation.

©2010 Optical Society of America

OCIS codes: (300.6495) Terahertz spectroscopy; (160.4670) Optical materials; (160.4670) Optical properties.

References and links

1. J. Liu, and X.-C. Zhang, "Birefringence and absorption coefficients of alpha barium borate in terahertz range," J. Appl. Phys. **106**(2), 023107 (2009).
2. X.-C. Zhang, X. F. Ma, Y. Jin, T.-M. Lu, E. P. Boden, P. D. Phelps, K. R. Stewart, and C. P. Yakymyshyn, "Terahertz optical rectification from a nonlinear organic crystal," Appl. Phys. Lett. **61**(26), 3080–3082 (1992).
3. F. Pan, G. Knöpfle, C. Bosshard, S. Follonier, R. Spreiter, M. S. Wong, and P. Günter, "Electro-optic properties of the organic salt 4-N,N-dimethylamino-4'-N'-methyl-stilbazolium tosylate," Appl. Phys. Lett. **69**(1), 13–15 (1996).
4. C. Bosshard, R. Spreiter, L. Degiorgi, and P. Gunter, "Infrared and Raman spectroscopy of the organic crystal DAST: Polarization dependence and contribution of molecular vibrations to the linear electro-optic effect," Phys. Rev. B **66**(20), 205107 (2002).
5. A. Schneider, M. Neis, M. Stillhart, B. Ruiz, R. U. A. Khan, and P. Gunter, "Generation of terahertz pulses through optical rectification in organic DAST crystals: theory and experiment," J. Opt. Soc. Am. B **23**(9), 1822–1835 (2006).
6. T. Taniuchi, S. Okada, and H. Nakanishi, "Widely tunable terahertz-wave generation in an organic crystal and its spectroscopic application," J. Appl. Phys. **95**(11), 5984–5988 (2004).
7. H. Ito, K. Miyamoto, and H. Minamide, "Ultra-Broadband, Frequency-agile THz-wave Generator and its Applications," in *Advanced Solid-State Photonics, OSA Tech. Digest Ser.* (Nara, Japan, 2008), p. WD1.
8. J. Takayanagi, S. Kanamori, K. Suizu, M. Yamashita, T. Ouchi, S. Kasai, H. Ohtake, H. Uchida, N. Nishizawa, and K. Kawase, "Generation and detection of broadband coherent terahertz radiation using 17-fs ultrashort pulse fiber laser," Opt. Express **16**(17), 12859–12865 (2008).
9. M. Martin, J. Mangeney, P. Crozat, and P. Mounaix, "Optical phase detection in a 4-N,N-dimethylamino-4'-N'-methyl-stilbazolium tosylate crystal for terahertz time domain spectroscopy system at 1.55 µm wavelength," Appl. Phys. Lett. **97**(11), 111112 (2010).
10. T. Taniuchi, S. Ikeda, Y. Mineno, S. Okada, and H. Nakanishi, "Terahertz properties of a new organic crystal, 4'-dimethylamino-*N*-methyl-4-stilbazolium *p*-chlorobenzenesulfonate," Jpn. J. Appl. Phys. **44**(29), L932–L934 (2005).
11. T. Matsukawa, Y. Takahashi, R. Miyabara, H. Koga, H. Umezawa, I. Kawayama, M. Yoshimura, S. Okada, M. Tonouchi, and Y. Kitaoka, "Development of DAST-derivative crystals for terahertz wave generation," J. Cryst. Growth **311**(3), 568–571 (2009).
12. M. Yoshimura, T. Matsukawa, Y. Takemoto, K. Takeya, Y. Takahasi, H. Umezawa, S. Okada, M. Tonouchi, Y. Kitaoka, and Y. Mori, "New organic nonlinear optical crystal BDAS-TP for terahertz applications," in *Conference on Lasers and Electro-Optics* (San Jose, Ca., 2010), p. CTuR6.
13. K. Akiyama, S. Okada, Y. Goto, and H. Nakanishi, "Modification of DAST-based compounds toward enhanced terahertz-wave generation," J. Cryst. Growth **311**(3), 953–955 (2009).
14. M. Walther, K. Jensby, S. R. Keiding, H. Takahashi, and H. Ito, "Far-infrared properties of DAST," Opt. Lett. **25**(12), 911–913 (2000).

15. S. Ohno, K. Miyamoto, H. Minamide, and H. Ito, "New method to determine the refractive index and the absorption coefficient of organic nonlinear crystals in the ultra-wideband THz region," Opt. Express **18**(16), 17306–17312 (2010).
16. X. Zheng, C. V. McLaughlin, P. D. Cunningham, and L. M. Hayden, "Organic broadband terahertz sources and sensors," J. Nanoelectron. Optoelectron. **2**(1), 58–76 (2007).
17. C. V. McLaughlin, L. M. Hayden, B. Polishak, S. Huang, J. Luo, T. D. Kim, and A. K. Y. Jen, "Wideband 15 THz response using organic electro-optic polymer emitter-sensor pairs at telecommunication wavelengths," Appl. Phys. Lett. **92**(15), 151107 (2008).
18. K. Suizu, T. Shibuya, H. Uchida, and K. Kawase, "Prism-coupled Cherenkov phase-matched terahertz wave generation using a DAST crystal," Opt. Express **18**(4), 3338–3344 (2010).
19. X. Xie, J. Dai, and X.-C. Zhang, "Coherent control of THz wave generation in ambient air," Phys. Rev. Lett. **96**(7), 075005 (2006).
20. K. Y. Kim, J. H. Glownia, A. J. Taylor, and G. Rodriguez, "Terahertz emission from ultrafast ionizing air in symmetry-broken laser fields," Opt. Express **15**(8), 4577–4584 (2007).
21. M. Kress, T. Löffler, S. Eden, M. Thomson, and H. G. Roskos, "Terahertz-pulse generation by photoionization of air with laser pulses composed of both fundamental and second-harmonic waves," Opt. Lett. **29**(10), 1120–1122 (2004).
22. L. Duvillaret, F. Garet, and J. L. Coutaz, "A reliable method for extraction of material parameters in terahertz time-domain spectroscopy," IEEE J. Sel. Top. Quantum Electron. **2**(3), 739–746 (1996).
23. P. U. Jepsen, and B. M. Fischer, "Dynamic range in terahertz time-domain transmission and reflection spectroscopy," Opt. Lett. **30**(1), 29–31 (2005).
24. T. Vijayakumar, I. H. Joe, C. P. R. Nair, M. Jazbinsek, and V. S. Jayakumar, "Electron-phonon coupling and vibrational modes contributing to linear electro-optic effect of the efficient NLO chromophore 4-(*N,n*-dimethylamino)-*N*-methyl-4'-toluene sulfonate (DAST) from their vibrational spectra," J. Raman Spectrosc. **40**(1), 52–63 (2009).
25. D. G. Allis, J. A. Zeitler, P. F. Taday, and T. M. Korter, "Theoretical analysis of the solid-state terahertz spectrum of the high explosive RDX," Chem. Phys. Lett. **463**(1-3), 84–89 (2008).

1. Introduction

Recent advances in terahertz (THz) generation from air plasmas has allowed for broadband THz time-domain spectroscopy (TDS) of materials useful for THz emission and detection [1]. This new capability calls for the re-examination of materials of interest whose properties were previously studied over a very narrow band. The organic EO crystal 4-*N,N*-dimethylamino-4'-*N*'-methyl stilbazolium tosylate (DAST) has drawn attention as a THz emitter since 1992 [2] due to its large nonlinearity. A wealth of work has been conducted by the Gunter group on the nonlinear optical [3] and far-infrared properties [4] of DAST and its applicability as a THz emitter at long pump wavelengths [5]. DAST has also drawn recent interest as a tunable source of high power THz radiation spanning a very broad bandwidth using difference frequency mixing of two lasers [6–8]. Very recently, it has also been used for free-space electro-optic sampling (FSEOS) of broadband THz pulses [9]. The success of DAST as a bright, broadband THz source has led to a recent resurgence of research on organic crystalline THz emitters in general, many of which are DAST derivatives with similar chemical structures and optical properties [10–13].

The optimal use of DAST, or any other material, for THz applications requires accurate knowledge of the dielectric properties across the THz band. A previous TDS study of DAST with bandwidth up to 3 THz identified a strong absorption near 1.1 THz, which exceeded their available dynamic range [14]. A later study showed bandwidth from 1.3 - 4 THz [5], but the available dynamic range made clear identification of the absorption feature associated with the 3.1 THz feature difficult. In that study, DAST was used as the THz emitter and sensor, further complicating analysis as the absorption features present in the DAST sample will be precisely where the dynamic range is smallest. The refractive index of DAST has been recently calculated from Fourier Transform Infrared (FTIR) spectroscopy, which relies on Kramers-Kronig approximations [7]. More recently, the THz properties of DAST were estimated by modeling the THz emission from difference frequency generation (DFG) in DAST [15]. As DAST is capable of producing broadband THz radiation [8,16–18], precise measurements of the THz properties across a broader bandwidth is essential to determining the optimum operational parameters.

Though DAST is a monoclinic crystal of point group *m* with 10 non-zero electro-optic coefficients, only four are larger than 1 pm/V [3]. Typically, crystals are produced in the *ab*-plane. For light polarized along the *a*- or *b*-axis the THz emission via optical rectification (OR) will be polarized along the *a*-axis [16]. For this reason, it is important to know the THz refractive index along the *a*-axis of DAST. On the other hand, incident light with an arbitrary polarization in the *ab*-plane will result in a THz polarization along both the *a*- and the *b*-axis. Few studies have examined the THz properties of both crystallographic axes.

2. Results and discussion

We used a 150 mm focal length lens to focus 1 mJ, 45-fs, 800 nm pulses through a 100 μm thick type-I *β*-barium borate crystal to form a filament for air-plasma THz generation via mixing of the fundamental and second harmonic [19]. Though the precise mechanism of THz generation in ionized-air plasmas is a current subject of debate [20,21], air plasmas nonetheless provide bright sources of broadband THz radiation. A 100 μm thick 26 pm/V 40%-Lemke / 60%-APC poled polymer sensor [16] enabled detection of continuous bandwidth up to 12 THz without the need to form a secondary plasma for detection. THz TDS was performed on a 160 μm thick 2.5 mm x 1.8 mm DAST crystal (Rainbow Photonics) oriented such that the THz polarization was incident upon either the *a*-axis or the *b*-axis of the sample. An iris was placed directly in front of the sample and closed so that the THz radiation only sampled the DAST crystal. As a reference, the transmission through the unobstructed iris was measured [Fig. 1(a), black line]. The iris had little effect on the overall THz amplitude, as the focused spot size was about 800 μm. The THz transmission through the *a*-axis of the DAST sample [Fig. 1(a), red line] shows five distinct features over this bandwidth at 1.1, 3.1, 5.2, 7.1, 8.4, and weak absorptions at 11, and 12.3 THz. When DAST is used as a THz emitter, these same features are observed [6,8,16–18]. Transmission through the *b*-axis [Fig. 1(b), red line] shows seven features centered at 1.1, 1.3, 1.6, 3.0, 5.2, 7.2, and 9.6 THz and a weak absorption at 11.7 THz.
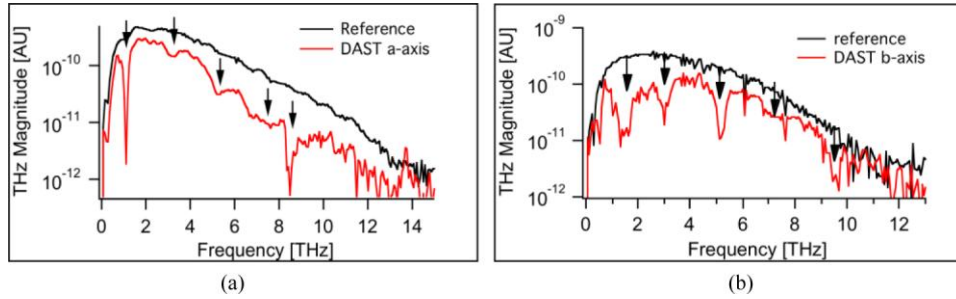
Fig. 1. THz transmission through an unobstructed iris (black) and (a) corresponding transmission through the *a*-axis of a 160 μm thick DAST crystal (red). There are absorption features centered at 1.1, 3.1, 5.2, 7.1, and 8.4 THz (arrows). (b) The transmission through the *b*-axis shows absorption features centered at 1.1, 1.3, 1.6, 3.0, 5.2, 7.2, and 9.6 THz (arrows).

We modeled the transmission through an optically thick monolithic sample as,

$$\tilde{T}(v) = \frac{2\tilde{n}_2(v)\big(\tilde{n}_1(v)+\tilde{n}_3(v)\big)}{\big(\tilde{n}_1(v)+\tilde{n}_2(v)\big)\big(\tilde{n}_2(v)+\tilde{n}_3(v)\big)} e^{-i(\tilde{n}_2(v)-\tilde{n}_1(v))l_2\omega/c}, \tag{1}$$

where $\omega \equiv 2\pi v$, *c* is the speed of light, l_2 is the thickness of the sample, and $\tilde{n}_2(v)$, $\tilde{n}_1(v)$, and $\tilde{n}_3(v)$ are the frequency-dependent complex indices of refraction of the sample and the mediums before and after it respectively. By minimizing the error function proposed by Duvillaret et al. [22] the index of refraction and absorption coefficients were determined. Unfortunately, the measured absorption features near 8.4 & 12.3 THz for the *a*-axis and 9.6 &

11.7 THz for the *b*-axis slightly exceed the maximum measureable absorption coefficient as defined by the dynamic range [23]. However, it is still clear that five distinct absorption bands exist in the data for the *a*-axis and seven for the *b*-axis. Despite the numerous absorption bands, the THz refractive index of the *a*-axis of DAST is relatively flat across the band after the large feature at 1.1 THz.

(a)   (b)
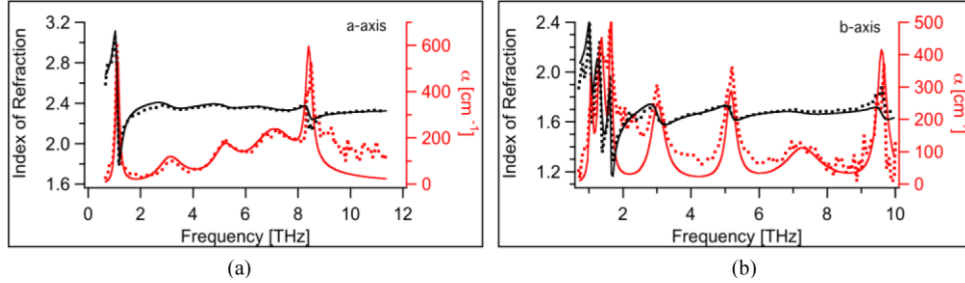
Fig. 2. The measured index of refraction (black dots) and power absorption coefficient (red dots) of (a) the *a*-axis and (b) the *b*-axis of DAST from 0.6 to 10 THz. The solid lines are fits to the Lorentz oscillator model described in the text.

The dielectric function can be modeled using a collection of Lorentz oscillators,

$$\tilde{\varepsilon}(\omega) = \varepsilon_{EL} + \sum_j \frac{\varepsilon_{ST_j} \Omega_j^2}{\left(\Omega_j^2 - \omega^2\right) - 2i\gamma_j \omega},\tag{2}$$

where ε_{EL} is the background dielectric constant, Ω_j is the resonance frequency, ε_{ST_j} describes the oscillator strength, and γ_j is the line width. The sum is taken over the number of resonant features, five in the case of the *a*-axis and seven for the *b*-axis of DAST. Equation (2) is fit to the measured complex dielectric function $\tilde{\varepsilon}(\omega) = \left(n(\omega) + 2ic\alpha(\omega)/\omega\right)^2$, where *c* is the speed of light and *α* is the power absorption coefficient. To recover the index of refraction and absorption coefficient, given $\tilde{\varepsilon}(v) = \varepsilon_1(v) + i\varepsilon_2(v)$, we use the relations

$$n(v) = \sqrt{\frac{\sqrt{\varepsilon_1^2(v) + \varepsilon_2^2(v)} + \varepsilon_1(v)}{2}} \quad \alpha(v) = \frac{2\omega}{c}\sqrt{\frac{\sqrt{\varepsilon_1^2(v) + \varepsilon_2^2(v)} - \varepsilon_1(v)}{2}}.\tag{3}$$

(a)   (b)
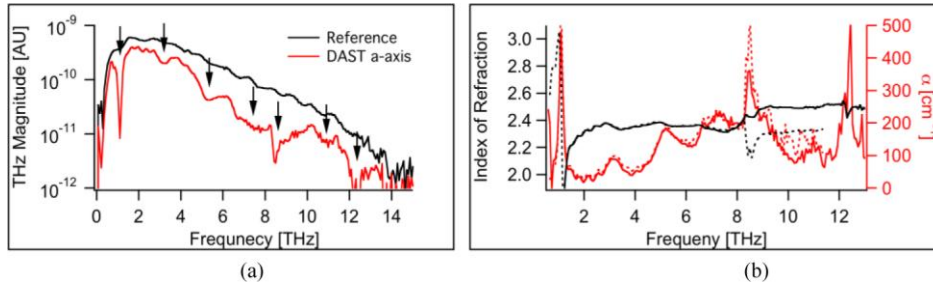
Fig. 3. (a) Broader bandwidth THz spectroscopy clearly identifying seven absorption bands. (b) The new data set (solid) overlaps previous data (dashed) but experiences an artificial kink in the index of refraction at the 8.4 THz absorption feature, due to the saturation of this absorption feature.

The fit to the *a*-axis absorption fails to accurately represent the data at high frequencies, Fig. 2. One possibility is that absorption features at frequencies >10 THz, which are not above the noise floor of this measurement, influence the absorption data over this range. To investigate this possibility, the bandwidth of the THz spectrometer was optimized, revealing

features near 11 & 12.3 THz, Fig. 3(a). Unfortunately, the absorption feature near 8.4 THz far exceeded the dynamic range of our spectrometer for this case, saturating the measured absorption, Fig. 3(b). This saturation led to a corresponding anomalous distortion of the THz phase and thus the index of refraction. However, there is excellent agreement with the previous THz measurements over the remaining frequency range. As only the data at the distortion is affected, the higher frequency refractive index data remains valid. This higher frequency data can be shifted to the values it would have assumed if not for the distortion, which will agree with previous measurements across the overlapped frequency range, and can be appended to the end of the previous measurement. The resulting composite refractive index and absorption traces, Fig. 4, can be modeled over a broader frequency range to achieve more accurate fits. Similar methods are used to generate composite traces of the refractive index and absorption coefficient of the *b*-axis of DAST.
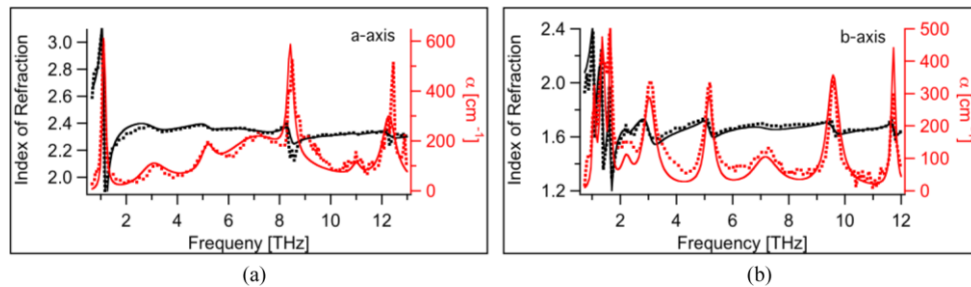
Fig. 4. Composite refractive index and absorption coefficient of the (a) *a*- and (b) *b*-axis of DAST from 0.6 – 12 THz. The solid lines are fits to the Lorentz oscillator model described in the text.

Table 1. Fit parameters of DAST dielectric function to Lorentz oscillator model

DAST *a*-axis $\varepsilon_{EL} = 5.48$		
Oscillator Frequency $\omega/2\pi$ [THz]	Oscillator Strength	Line Width [THz]
1.1	0.79	0.39
3.1	0.15	4.2
5.2	0.03	1.9
7.1	0.16	11
8.4	0.02	0.85
11	0.002	1.3
12.3	0.01	2.1
DAST *b*-axis $\varepsilon_{EL} = 2.81$		
Oscillator Frequency $\omega/2\pi$ [THz]	Oscillator Strength	Line Width [THz]
1.1	0.27	0.31
1.3	0.43	0.84
1.6	0.10	0.20
2.2	0.05	1.3
3	0.12	1.6
5.2	0.03	1.1
7.2	0.02	3.4
9.6	0.02	1.7
11.7	0.004	5.2

The fit results are summarized in Table 1. We identify resonances centered at 1.1, 3.1, 5.2, 7.1, 8.4, 11, and 12.3 THz for the *a*-axis of DAST. The resonances at 1.1 and 3.1 THz are similar in center frequency and line width to those reported by Schneider, et al. [5] The higher frequency features have previously been observed via FTIR [7], Raman spectroscopy [24], or in THz emission from DAST [6,17] but the associated linewidths and indices of refraction were not given. The feature at 1.1 THz has been previously attributed to a transverse optical phonon associated with the anion-cation pair vibration [14]. Isolated, single molecule, gas

phase density functional theory (DFT) models have attributed the feature at 3.1 THz to the vibration of the anion, at 5.2 THz to a vinyl C-H torsional mode on the cation, and at 12.3 THz to a phenyl ring mode [24], but fail to predict the other absorption features. DFT models such as these have difficulty reproducing low frequency THz spectra, which are dominated by collective vibrations, since they neglect inter-molecule interactions that are present in the bulk. Modeling THz spectra remains an active area of research [25]. The similar structure of the derivatives of DAST will give them similar absorption features [10]. Though Cherenkov radiation from DAST may avoid phase matching requirements, the absorption features remain present in the emitted spectrum [18]. Estimating the THz properties of DAST by modeling its emission via DFG underestimates the effects of these absorption features [15]. Such techniques are valuable above 15 THz where TDS is difficult. We also identify resonances centered at 1.1, 1.3, 1.6, 2.2, 3, 5.2, 7.2, 9.6 and 11.7 THz for the *b*-axis of DAST. Only the resonances at 1.1, 1.3, and 1.6 have been previously observed [14], though DFT models assign the 11.7 THz feature to the torsional mode of the anion methyl group [24].

Given the optical properties of DAST [3], and THz indices we have determined, we compute the coherence length, l_c, across the band for various pump wavelengths, Fig. 5. For Ti:Sapphire wavelengths the l_c is larger for an emitter beam polarized parallel to the *b*-axis than the *a*-axis. This is unfortunate, as the nonlinearity is nearly an order of magnitude larger for *a*-axis emission. Though the emission could be stronger for *a*-axis orientation, the *b*-axis must be used if broad bandwidth is desired. The bandwidth over which there is good phase matching is consistent with the bandwidth seen from a 60 μm thick DAST crystal [16]. The largest component of the nonlinear susceptibility, χ_{111}, can be accessed at longer wavelengths. There is good phase matching near 1300 nm for light polarized parallel to the *a*-axis. Unfortunately, the nonlinear susceptibility exhibits dispersion, as the linear absorption bands of DAST are near 500 nm. At longer wavelengths the nonlinearity is no longer resonantly enhanced and will be lower than at shorter wavelengths. Though the coherence length is large at these wavelengths, thick DAST crystals used as THz emitters will show numerous spectral gaps due to phonon absorption. The coherence length is consistent with the near 15 THz bandwidth reported using a 160 μm thick DAST crystal [17].
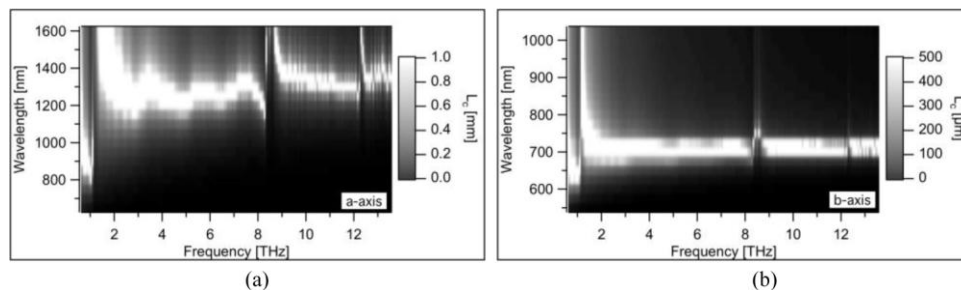
Fig. 5. The coherence length, l_c, across the THz band of a DAST emitter pumped with (a) *a*-axis or (b) *b*-axis polarized light at relevant wavelengths.

In summary, we have reported the first use of a THz spectrometer based on air-plasma THz generation and FSEOS in a poled polymer. The far infrared properties of DAST are measured from 0.6 to 12 THz, identifying multiple previously unidentified phonon bands and showing their effect on THz emission. Our results are consistent with recent published FTIR spectra [7] and broadband THz emission spectra from DAST [17], and can be used to guide future THz applications.

Acknowledgements